Keisuke Yano[1] and Masayuki Kano[2]

[1] Institute of Statistical Mathematics, 10-3 Midori cho, Tachikawa City, Tokyo 190-8562, Japan.

[2] Graduate School of Science, Tohoku University, 6-3 Aramaki-aza-aoba, Aoba-ku, Sendai, 980-8578, Japan.

Corresponding author: Keisuke Yano (yano@ism.ac.jp)

Key Points:

- We developed a sparse estimation detection method for short-term slow slip events based on a Global Navigation Satellite System array. (134 characters)
- Synthetic tests revealed that slow slip events can be detected with our method and the onset of events can be accurately determined. (132 characters)
- Our method was applied to real data from the array at the Nankai subduction zone in Southwest Japan and identified new events. (126 characters)

Abstract

The discovery of slow slip events (SSEs) based on the installation of dense geodetic observation networks has provided important clues to understanding the process of stress release and accumulation in subduction zones. Because short-term SSEs (S-SSEs) do not often result in sufficient displacements that can be visually inspected, refined automated detection methods are required to understand the occurrence of S-SSEs. In this study, we propose a new method based on which S-SSEs can be detected in observations derived by a Global Navigation Satellite System (GNSS) array by using l_1 trend filtering, a variation of sparse estimation, in conjunction with combined p-value techniques. The sparse estimation technique and data-driven determination of hyperparameters are utilized in the proposed method to identify candidates of S-SSE onsets. In addition, combined p-value techniques are used to provide confidence values for the detections. The results of synthetic tests demonstrated that almost all events can be detected with the new method, with few misdetections, compared with automated detection methods based on Akaike's information criteria. The proposed method was then applied to daily displacements obtained at 39 GNSS stations in the Nankai subduction zone in western Shikoku, southwest Japan. The results revealed that, in addition to all known events, new events can be detected with the proposed method. Finally, we found the number of low-frequency earthquakes in the target region increased around at the onsets of potential events. (243 words)

Plain language summary

Slow slip events characterized by a slower fault rupture compared to regular earthquakes have been discovered in tectonic zones worldwide and have helped

us understand the surrounding stress environment including megathrust zone. This study focuses on short-term SSEs (S-SSEs) with a duration of several days. S-SSEs have been observed by a Global Navigation Satellite System (GNSS) array, but do not often result in sufficient displacements that can be visually detected. So, refined detection methods have become necessary. We present a new automated detection method of S-SSE using a GNSS array. Our method utilizes $l1$ trend filtering, a sparse estimation technique, and combined p-value techniques to provide not only candidates of S-SSEs but also confidence values for detections. The synthetic tests showed that our method successfully detect almost all events with few misdetections. The application to real data in the Nankai subduction zone in western Shikoku, southwest Japan, revealed our method detected new potential events in addition to all known events. (160 words)

1 Introduction

Slow slip events (SSEs) have been observed in many subduction zones in which megathrust earthquakes occur using geodetic instruments (Schwartz & Rokosky 2007; Beroza & Ide 2011; Obara & Kato 2016). During these events, which often occur at downdip extensions of strongly locked seismogenic zones on plate interfaces, accumulated interplate stress is released with over days to years. The surrounding stress environment is then perturbed and the events potentially affect the occurrence of megathrust earthquakes (c.f., Graham et al., 2014; Ito et al., 2013; Kato et al., 2012; Ozawa et al., 2012; Radiguet et al., 2016; Ruiz et al., 2014; Socquet et al., 2017; Voss et al., 2018; Yokota & Koketsu, 2015). Therefore, identifying SSEs is an important first step toward understanding megathrust earthquakes.

The visual inspection of observations based on the installation of dense geodetic observation networks, including tilt/strain meters and the Global Navigation Satellite System (GNSS), has led to the discovery of a large number of SSEs. For example, long-term SSEs (L-SSEs) with a duration ranging from 6 months to 5 years have been observed beneath the Bungo channel and in the Tokai region, Southwest Japan (Hirose et al., 1999; Ozawa et al., 2002). In addition, short-term SSEs (S-SSEs) with a recurrence interval of several months that last for several days have been discovered in these areas (Obara et al., 2004; Hirose & Obara 2005; Obara & Sekine, 2009). Discoveries of S-SSEs have also been reported in tectonic zones worldwide such as Cascadia (Dragert et al., 2001; Miller et al., 2002), Alaska (Ohta et al., 2006), New Zealand (Douglas et al., 2005; Wallace and Beavan 2006), and Guerrero, Mexico (Kostgrodov et al., 2003). In many cases, S-SSEs coexist with the tectonic tremors. The coupling phenomena between tectonic tremors and S-SSEs are referred to as episodic tremor and slip (ETS) events (c.f., Obara et al., 2004; Rogers & Dragert 2003; Payero et al., 2008).

Because S-SSEs do not often result in sufficient displacements that can be visually detected, refined detection methods have become necessary. The idea of using other types of slow fault slip phenomena have been discussed (Frank et

al., 2015; Bartlow 2020). Based on the assumption that S-SSEs occur in association with low-frequency earthquakes (LFEs), Frank et al. (2015) used LFE bursts as indicators for the occurrence of SSEs to select short time windows of GNSS data and stacked them. Based on this method, SSE-like signals along the average surface motion of all stacked events were successfully identified in Guerrero. The similar method was applied in the Nankai subduction zone to estimate the detailed spatial slip distributions (Kano et al., 2019; Kano & Kato 2020), and to characterize the crustal deformation caused by SSEs (Fujita et al., 2019). Bartlow (2020) added a spatial criterion to the method to accommodate larger study areas, such as Cascadia, and studied the time-averaged ETS slip rate at the interface of the Cascadia subduction plate.

However, according to the spatial studies of S-SSEs in Cascadia (Hall et al., 2018) and in southwest Japan (Kano et al., 2019; Kano & Kato 2020), not all S-SSEs coincide with LFE activities. Therefore, methods must be developed that can be used to detect S-SSEs based on GNSS data alone. In addition, as the stacking of GNSS time series potentially prevents the understanding of the spatiotemporal differences between individual S-SSEs, detection methods without stacking the original GNSS time series are preferable. Several such automated detection methods have been proposed. To determine whether an offset representing the occurrence of an S-SSE exists in sliding windows of a given window time length in a GNSS time series, Nishimura et al. (2013) utilized the difference of Akaike's information criteria (AIC; Akaike 1974), AIC, of a model assuming the existence of an offset and the model without such an assumption, and stack them over neighboring stations (stacked AICs). Based on this method, 207 S-SSEs along the Nankai Trough that occurred from 1996 to 2012 (Nishimura et al., 2013), 223 S-SSEs along the Ryukyu Trench that occurred from 1997 to 2013 (Nishimura 2014), and 176 S-SSEs in the Kanto and Tokai regions (Nishimura 2020) were successfully identified. Rousset et al. (2017) developed a geodetic matched filter, which creates SSE templates by utilizing a source function multiplied by Green's functions for a discretized fault and the correlation between templates and post-processed GNSS data and identified 28 SSEs that occurred from 2005 to 2014 in Guerrero.

In this study, we propose an approach utilizing l_1 trend filtering in conjunction with combined p-values for the automated detection of S-SSEs using a GNSS array. The l_1 trend filtering (Kim et al., 2009) is a type of sparse estimation that produces piecewise linear trend estimates without prior knowledge of the knot locations based on which the cutting of time series into fixed-length sliding time windows can be avoided and any specific template can be used for slip deformations. We modeled the GNSS time series along the plate motion and detected candidates for the start and end points of S-SSEs as knots of l_1 trend filtering. Sparse estimation, including l_1 trend filtering, has recently been utilized in seismology (c.f., Loris et al., 2007; Klinger 2010; Yao et al., 2011; Evans & Meade, 2012; Nakata et al., 2016; Nakata et al., 2017; Hirose et al., 2020). In most studies, it has been used to improve the spatial resolution of the inversion analysis in the presence of sharp discontinuities. An exception is the work of

Klinger (2010) who used l_1 trend filtering to segment strike-slip earthquake surface ruptures. We employed a sparse estimation technique for the change point detection in GNSS time series.

We examined the validity of the proposed method by using a synthetic dataset in comparison with the automated detection method proposed by Nishimura et al. (2013). The comparison showed that our method yielded a better detection rate and small false positive rate. We also applied our method to real data from the GNSS array of the GNSS Earth Observation Network System (GEONET) in the Nankai subduction zone, Southwest Japan. Subsequently, we conducted inversion analysis using the Markov chain Monte Carlo (MCMC) method to analyze and discuss the occurrence of new potential events and their relation to LFEs.

2 Data

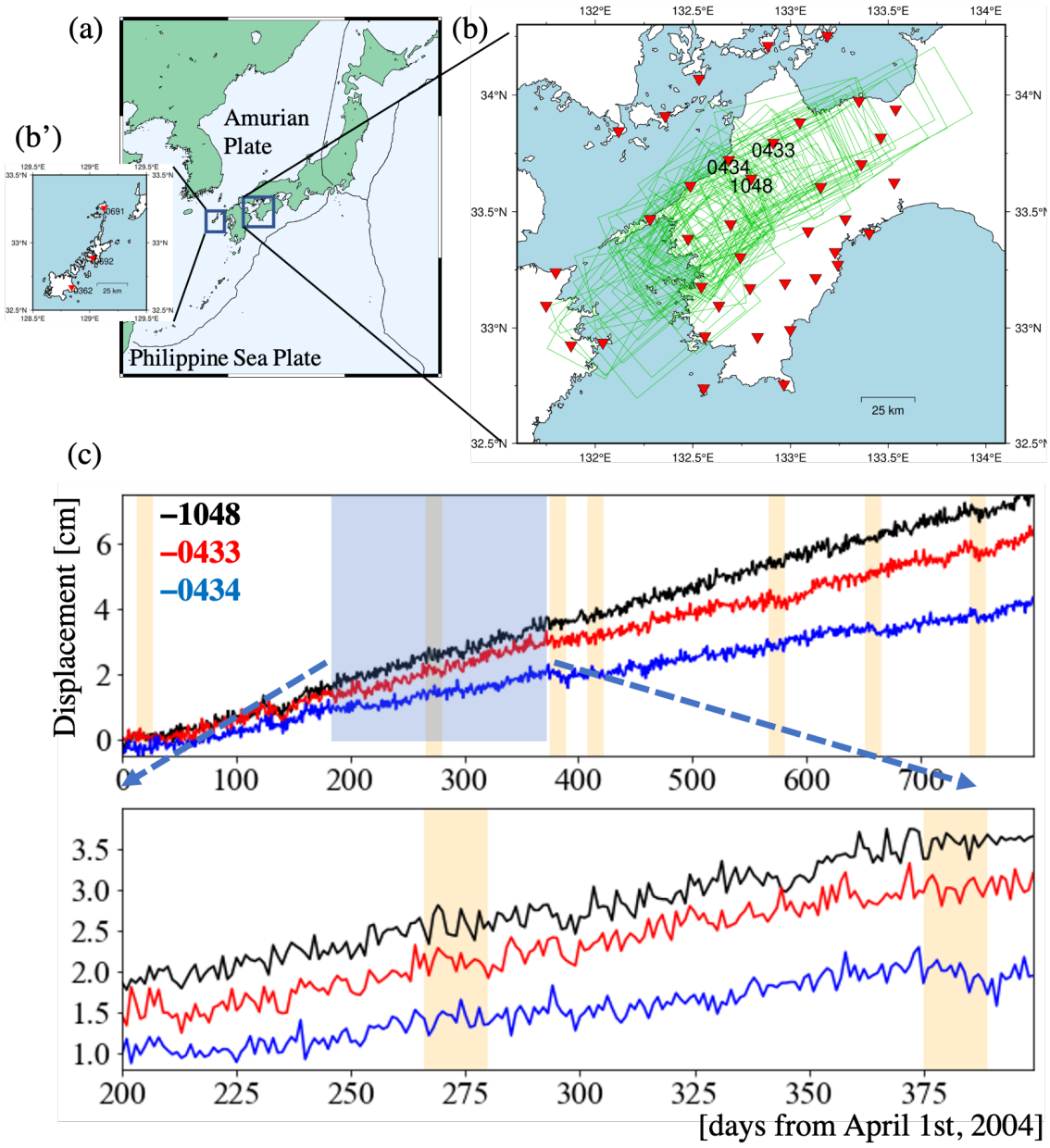

Figure 1. Map of the study area. **(a)** Tectonic setting around western Shikoku Island in Southwest Japan. **(b)** Map of GNSS stations (inverted red triangles) used in this study with the fault locations of known S-SSEs (green rectangles) from Sekine et al. (2010) and Nishimura et al. (2013). **(b')** Map of GNSS stations on the Goto

Islands. **(c)** The N45°W component of the GNSS time series at station 0434 for 800 days starting on April 1, 2004. Onsets ±7 days of known S-SSE catalogs (Sekine et al., 2010; Nishimura et al., 2013) are shaded in orange. **(d)** Enlarged time series obtained on the 200th day.

In this study, we used daily GNSS time series from 39 GEONET stations in the Nankai subduction zone beneath western Shikoku Island in Southwest Japan (Figure 1) derived from the GEONET F3 solution by the Geospatial Information Authority of Japan (Nakagawa et al., 2009). In this region, the Philippine Sea Plate is subducting beneath the Amurian Plate and large megathrust earthquakes with a moment magnitude (M_w) $\sim$ 8 have ruptured shallow parts of the plate interface at intervals of 90–200 years (Ando 1975). The 1944 M_w 8.1 Tonankai earthquake and 1946 M_w 8.3 Nankai earthquake (Sagiya and Thatcher 1999; Baba et al., 2002, 2006) are the most recent ones. In the deep transition zone at depth of ~35km, S-SSEs were often detected by GNSS or tilt meters (Figure 1b; Sekine et al., 2010; Nishimura et al., 2013). We used a period of 800 days, from April 1, 2004, to June 11, 2006.

We calculated the relative displacements with respect to the average time series of three stations on the Goto Islands (Figure 1b') to remove common model errors (Kano et al., 2019). Two horizontal displacements at each GNSS station were projected onto the N45°W direction, which is the direction of the motion of the Philippine Sea Plate relative to the Amurian Plate. We expected that the SSE signals along this direction will be large. Figure 1c shows an example of the GNSS time series obtained at stations 1048, 0433, and 0434. When an S-SSE occurs, the time series generally moves in the opposite direction of the steady movement; see the displacements at station 0434 from days 375 to 385.

3 Methods

In this study, an approach utilizing l_1 trend filtering, a variation of sparse estimation, in conjunction with combined p-values is proposed for the automated detection of S-SSEs using a GNSS array. A schematic flow of the proposed method is shown in Figure 2. First, we applied l_1 trend filtering to the GNSS time series at all stations. We then identified candidates for S-SSE occurrences. Finally, we calculated the confidence values for the S-SSE detection. The details of each procedure are described in the following subsections.

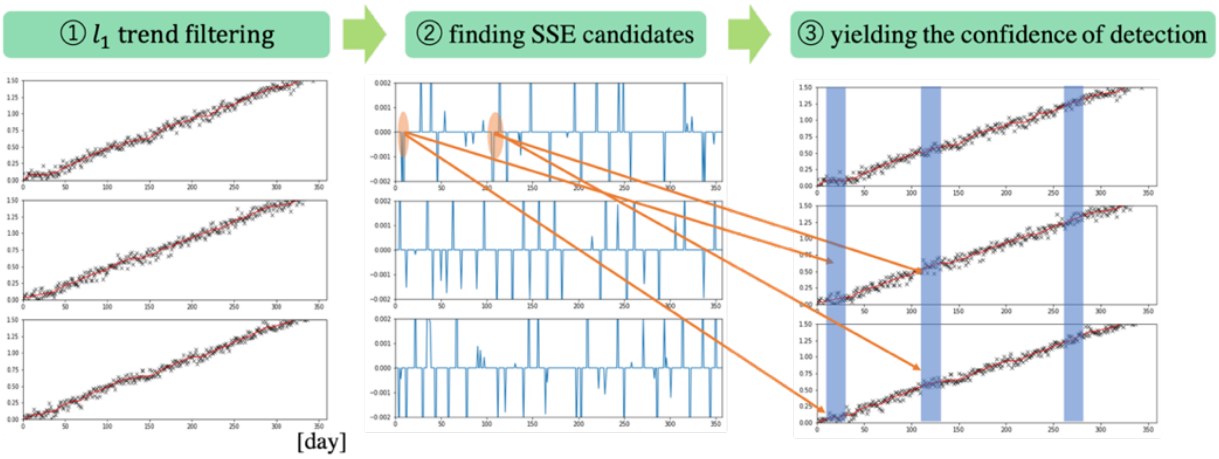

Figure 2. Outline of the proposed method.

3.1 l_1 trend filtering

First, we applied l_1 trend filtering to the GNSS time series at all stations. Let $\{X_t^s : t = 1, \dots, T\}$ be a (projected) GNSS time series of length T at station s, l_1 trend filtering $\{\widehat{X}_t^s : t = 1, \dots, T\}$ of this series with hyperparameter $\lambda > 0$ can be obtained by minimizing

$$\sum_{t=1,\dots,T} (X_t^s - \theta_t)^2 + \lambda \sum_{t=1,\dots,T-2} |(\theta_{t+2} - \theta_{t+1}) - (\theta_{t+1} - \theta_t)| \quad (1)$$

with respect to a sequence $\{\theta_t \in \mathbb{R} : t = 1, \dots, T\}$. Here, the first term of Eq. (1) represents the misfit and the second term of Eq. (1) represents the degree of violating the constraint that the first-order differences $\{\theta_{t+1} - \theta_t : t = 1, \dots, T-1\}$ are piecewise constant.

The l_1 trend filtering for any $\lambda > 0$ is known to be piecewise linear without prior determination of locations of knots (breaks at which the slopes change); see Section 3 in Kim et al. (2009). As λ increases, the number of knots increases. As λ decreases, the number of knots decreases. This hyperparameter λ can be determined by minimizing Mallows' C_p (Mallows 1973; Tibshirani & Taylor 2012; Tibshirani 2014), which is defined as follows:

$$C_p(\lambda) = \sum_{t=1,\dots,T} \frac{\left(X_t^s - \widehat{X}_t^s\right)^2}{\left(\sigma_s\right)^2} + \left\{\text{Number of knots in } \widehat{X}_t^s\right\} + 2, \quad (2)$$

where σ_s^2 is the noise variance at station s. When σ_s^2 is unknown, its estimate is plugged in. Mallows' C_p balances the misfit (first term on the right-hand side of Eq. (2)) and the number of knots (second term), that is, the number of segmentations of the fitted piecewise linear function. Therefore, l_1 trend filtering with Mallows' C_p can yield the piecewise linear fitting with data-driven determination of locations and the number of knots.

In real data applications, GNSS stations are divided into two groups (primary

and secondary stations) based on the behavior of C_p with respect to λ because not all GNSS time series can be fitted with a piecewise linear function. If a curve of $C_p(\lambda)$ with respect to λ displays a unique minimizer (implying that the piecewise linear function fits the target time series well), we call the target station primary; we call stations within 30 km from the primary station the secondary stations. In synthetic tests, we selected one arbitrary station as a primary station. The other stations were used as secondary stations because the stations of the synthetic tests did not differ.

3.2 Confidence of S-SSE detection

Subsequently, we employed (a) knots of l_1 trend-filtered time series at primary stations and (b) original time series at secondary stations to provide candidates for S-SSEs including the event duration and detection confidence.

We selected knots $\{T_i^s : i = 1, \dots, N\}$ with the number of knots N when the second-order difference in the l_1-trend-filtered time series, that is, $\widehat{X}^s_{T_i^s+1} - 2\widehat{X}^s_{T_i^s} + \widehat{X}^s_{T_i^s-1}$, was negative at a primary station s as candidates for the starting time of S-SSEs. A negative second-order difference is required because displacements caused by S-SSEs are expected to yield sign changes from positive to negative velocities. For each $i = 1, \dots, N$ and for each primary station s, we then defined D_i^s as the time difference between T_i^s and the first time at which $\widehat{X}^s_{t+1} - 2\widehat{X}^s_t + \widehat{X}^s_{t-1}$ at the primary station s becomes non-zero after T_i^s. We considered $\{D_i^s : i = 1, \dots, N\}$ as candidate values for the duration of S-SSEs.

By using $\{T_i^s : i = 1, \dots, N\}$ and $\{D_i^s : i = 1, \dots, N\}$, we conducted statistical hypothesis tests at secondary station s' and for each event candidate i of the null hypothesis that S-SSE does not occur at T_i^s. We express this null hypothesis as the condition under which

$$Z_i^{s'} = \frac{\hat{v}^{s'}_{\text{after},i} - \hat{v}^{s'}_{\text{global}}}{sd(\hat{v}^{s'}_{\text{after},i} - \hat{v}^{s'}_{\text{global}})}$$

is zero, where $\hat{v}^{s'}_{\text{after},i}$ is an estimate of the first-order differences of the GNSS time series at a secondary station s' during the period from T_i^s to $T_i^s + D_i^s$, $\hat{v}^{s'}_{\text{global}}$ is an estimate of the stationary slope of the GNSS time series at a secondary station s', and sd is the standard deviation. The parameter $\hat{v}^{s'}_{\text{global}}$ was calculated as follows: We applied the l_1 trend filter to the GNSS time series at station s' to obtain $\widehat{X}^{s'}_t$ and used the mean of $\left\{\widehat{X}^{s'}_{t_j+1} - \widehat{X}^{s'}_{t_j} : j = 1, \dots, J\right\}$ for all time steps $\{t_j : j = 1, \dots, J\}$ at which $\widehat{X}^{s'}_{t_j+1} - \widehat{X}^{s'}_{t_j} > 0$. The parameter $\hat{v}^{s'}_{\text{after},i}$ was calculated by least square fitting a linear function to $\{X^{s'}_{T_i^s}, \dots, X^{s'}_{T_i^s+D_i^s}\}$. Based on the assumption that $Z_i^{s'}$ follows the standard normal distribution when the change in

the first-order difference of the GNSS time series does not occur at T_i^s, the statistical hypothesis testing produces p-values, that is, $p_i^{s'} = \Pr\left(Z \leq Z_i^{s'}\right) = \Phi(Z_i^{s'})$, where $\Phi(\cdot)$ is the cumulative distribution function of the standard Gaussian distribution. If $p_i^{s'}$ approaches 0, rejecting the null hypothesis becomes more confident, implying that S-SSEs may occur at T_i^s with high confidence. If $p_i^{s'}$ approaches 1, accepting the null hypothesis becomes more confident, implying that S-SSEs may not occur at T_i^s.

Finally, we combine station-wise non-confidence values $\{p_i^{s'} : s' \in \text{secondary stations}\}$ by using the combined p-value technique (Good 1958; Wilson 2019): $p_{\mathrm{i}}^{-1} = \sum_{s'} \frac{1}{p_i^{s'}}$. This harmonic mean stacking produces a single robust value $\{p_i : i \in \text{candidates}\}$ with respect to the non-confidence of the S-SSE occurrence. By setting $\{\ \widetilde{p}_i = 1 - p_i : i \in \text{candidates}\}$, we obtain candidates for the S-SSE occurrence time including their confidence.

4. Synthetic test

In this section, we demonstrate the performance of our method by using synthetic data in comparison with the AIC-based S-SSE detector (Nishimura et al., 2013).

We created a synthetic dataset of multiple projected GNSS time series with a length of 730 days (2 years) as follows: For each station s, the value at time step t is given by:

$$X_t^s = v_0 t - \sum_{i=1,\ldots,N} \left\{ v_i^s \left(1 - \exp\left(-\frac{(t-t_i)}{\tau_i}\right)\right) H(t-t_i) \right\} + \sigma^s \varepsilon_t^s,$$

where $v_0^s > 0$ is the stationary velocity of the displacement of station s, N is the number of S-SSEs, and the function $v_i^s \left(1 - \exp\left(-\frac{(t-t_i)}{\tau_i}\right)\right) H(t-t_i)$ is the displacement caused by the i-th S-SSE starting at t_i with duration τ_i and magnitude v_i^s with the Heaviside step function $H(x)$. We set the number of stations to seven. We set the recurrence interval of S-SSEs to 30 days and then the whole time series contained 23 S-SSEs. We set the duration of each S-SSE to five days and the stationary velocity v_0 to 2/365 cm/day. The noise standard deviations σ^s were assigned to be 0.05, 0.07, 0.1, 0.04, 0.05, and 0.06 cm by referring to the noise variances of real data in Section 2. We set the strengths of SSEs observed at station v_i^s to 0.105, 0.04, 0.02, 0.07, 0.06, 0.05, and 0.04 cm by referring to the actual values of the S-SSE event on April 21, 2004. Figure 3a shows the sequence obtained at the primary station.

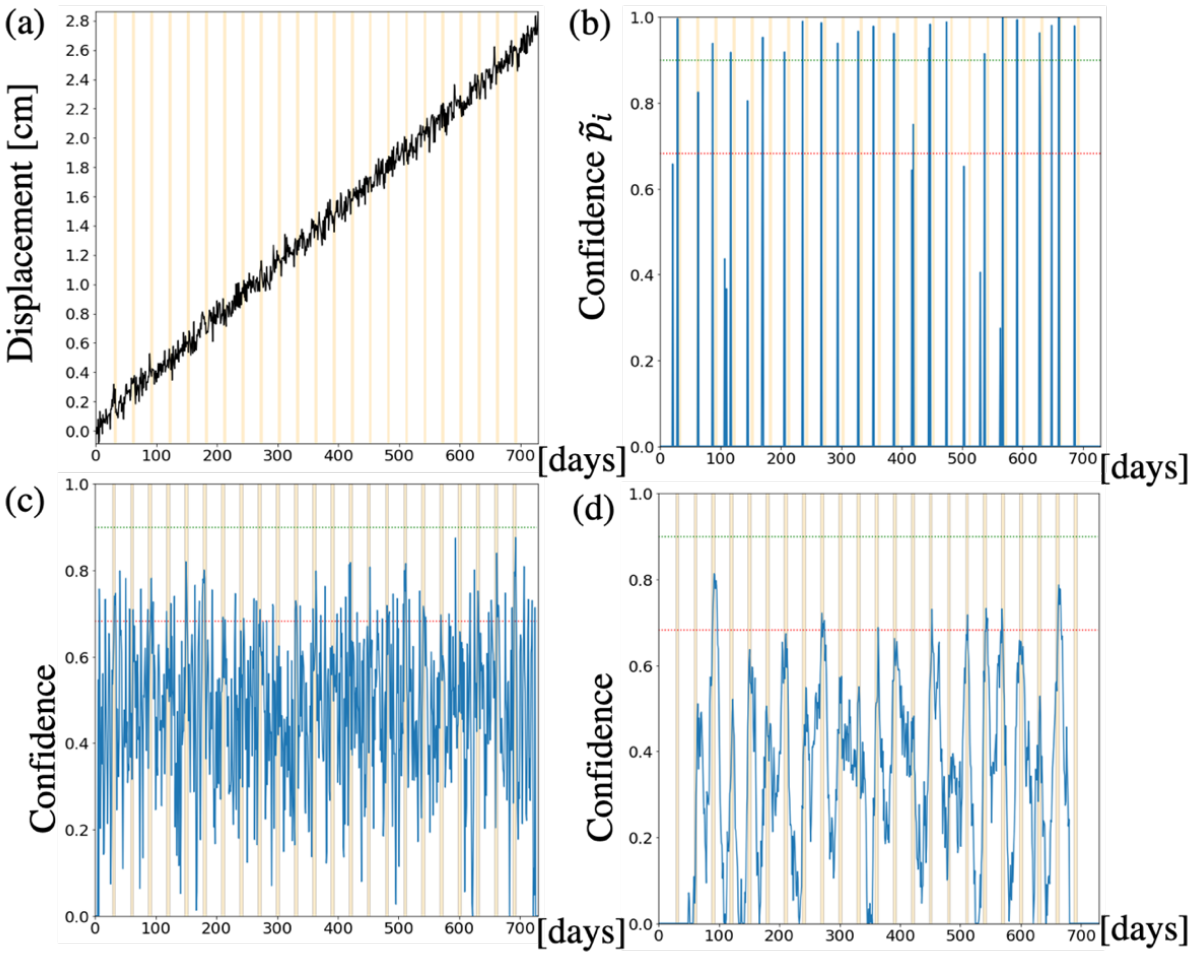

Figure 3. **(a)** Synthetic time series (colored in black) with S-SSEs (orange shades). **(b)** *S*equence of confidence $\tilde{p}_i$ including the values of zero-padded non-candidates. The 90% line is green. The 68% line is red. **(c)** Sequence of stacked ΔAICs (converted to probability values) with a window length of 10 days. **(d)** Sequence of stacked ΔAICs (converted to probability values) with a window length of 100 days.

We first discuss the performance of the proposed method. Figure 3b shows the sequence of confidence $\tilde{p}_i$ including the values of zero-padded non-candidates. Based on our method, 17 and 20 events were successfully detected, with a confidence greater than 0.9 and 0.68, respectively. Note that the threshold value of 0.68 is the value of $Pr(\Delta\text{AIC} \geq 0)$ with the AIC difference ΔAIC because the distribution of ΔAIC between two models with the number of parameters d and $d'(d < d')$ is the chi-square distribution with a degree of freedom $d^{'} - d$.

In contrast, our method yields three misdetections for both the 90% and 68% thresholds. Figure 3b also shows that, based on our method, confidence values are only assigned to the starting points of events, which implies that the starting points of S-SSEs can be accurately determined with our method. This may be because we employed an exponential function as the synthetic form of SSE deformation and the second derivative monotonically decreases.

Subsequently, we compared our method with that reported by Nishimura et al. (2013) based on which sliding windows with a fixed window length are produced and ΔAICs between two models are sequentially calculated: one model assumes an offset representing the occurrence of an S-SSE, whereas the other model does not. Finally, the sequences of ΔAIC over stations are stacked. A high stacked ΔAIC value indicates the existence of a S-SSE. Two window lengths ($L = 10$ and 100) were chosen for this comparison. For both window lengths, the stacked ΔAIC sequence did not produce confidence values above 0.9. For $L = 10$, all events are detected by this method, but many misdetections occur (Figure 3c). For $L = 100$, misdetections were not observed, but only eight events with confidence values above 0.68 were detected (Figure 3d). In general, the way of determining the optimal window length remains unclear. The results therefore show that our method can improve the method of ΔAIC stacking.

5 Application to real data

We applied our method to daily GNSS time series obtained at 39 GEONET stations in the Nankai subduction zone beneath western Shikoku Island in Southwest Japan, as described in Section 2. Seven S-SSEs occurred during the analysis period (Figure 4): the 4th and 7th events were discovered only by tiltmeters (Sekine et al., 2010); the 1st, 3rd, and 6th events were discovered only by GNSS; and the other events were discovered by both tiltmeters and GNSS (Nishimura et al., 2013).

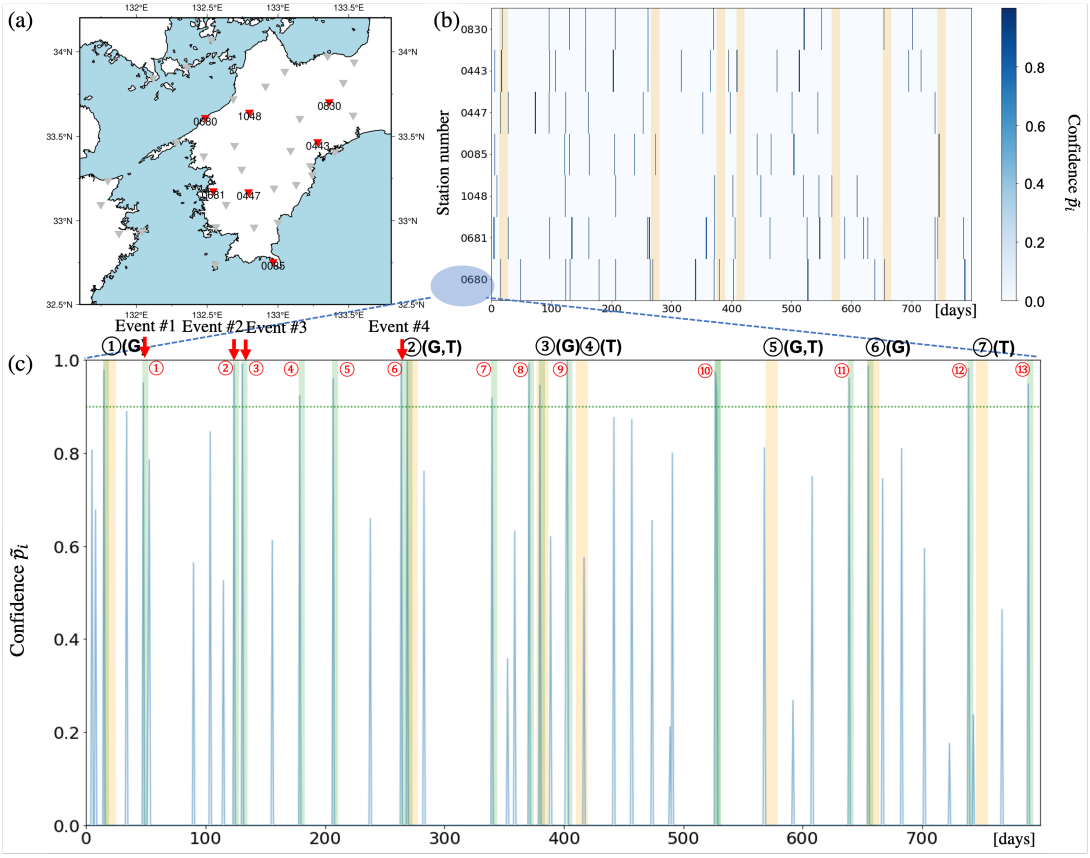

Figure 4. **(a)** Primary stations (red inverted triangles) with their station numbers. **(b)** Confidence values above 90% for all primary stations. Orange shades denote known S-SSEs (known onsets ± 7 *days*) based on Sekine et al. (2010) and Nishimura et al. (2013). **(c)** Sequence of confidence values at station 0680 (blue lines). The green dashed line denotes the threshold of 90%. The green shades represent periods of five days starting on the detected day. Each known SSE was numbered in black and marked with (G) or (T) if it was discovered by GNSS or tiltmeters, respectively. Otherwise, it is marked by (G,T). New potential events were numbered in red. The inversion results obtained for the four potential events marked with red arrows are shown in Figure 6.

Figure 4a represents the primary stations selected based on the behavior of Mallows' C_p. Note that the spatial distribution of the primary stations is not concentrated in specific regions. Figures 4b and c show the sequences of the confidence values at all primary stations and at a single station (station 0680), respectively. Figure 4b shows that all known S-SSEs (1st, 2nd, 3rd, 5th, and

6th event), which have been previously detected by GNSS, were successfully detected with our method. In addition, two S-SSEs (4th and 7th event) were detected, which had not been previously detected by GNSS. Figure 4c also shows that our method highlights the onsets of potential events only. Figure 4c suggests that, based on station 0680, our method reveals 13 events that have not been detected with other methods based on station 0680. These events are discussed below.

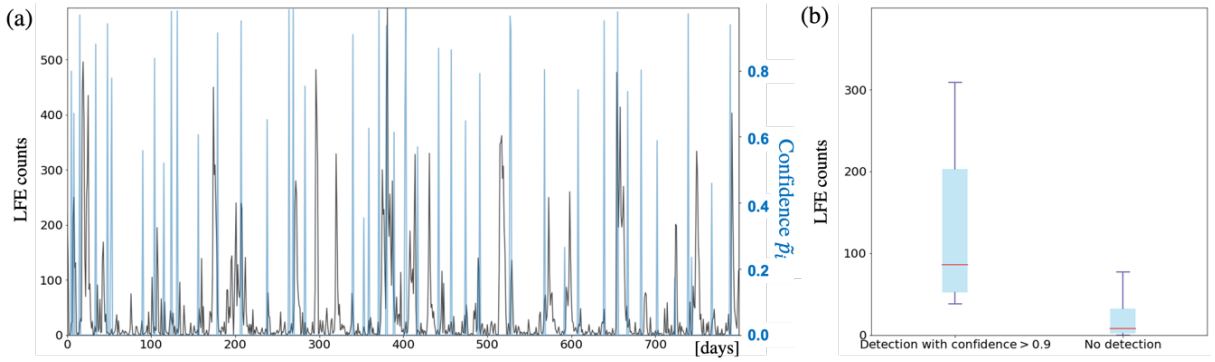

Figure 5. **(a)** Sequences of daily LFE counts (black line) and confidence values at station 0680 (blue line) starting on April 1, 2004. **(b)** Boxplot of LFE counts within intervals of six days around the detected days with a confidence above 0.9 and that outside these intervals. Mean values are shown in red.

We investigated new potential events detected by our method from the perspective of their correlation with the daily LFE counts. We used the LFE catalog for the Nankai subduction zone created by Kato and Nakagawa (2020) and extracted the LFEs around Shikoku Island (Figure 1b). The local peaks of daily LFE counts starting on April 1, 2004 are concordant with the sequence of confidence values at station 0680 (Figure 5a). This can be clearer by comparing the LFE counts within the intervals of six days around the detected days with a confidence above 0.9 and those outside these intervals (Figure 5b), showing that the LFE occurrences on the detected days are significantly larger than those on the other days.

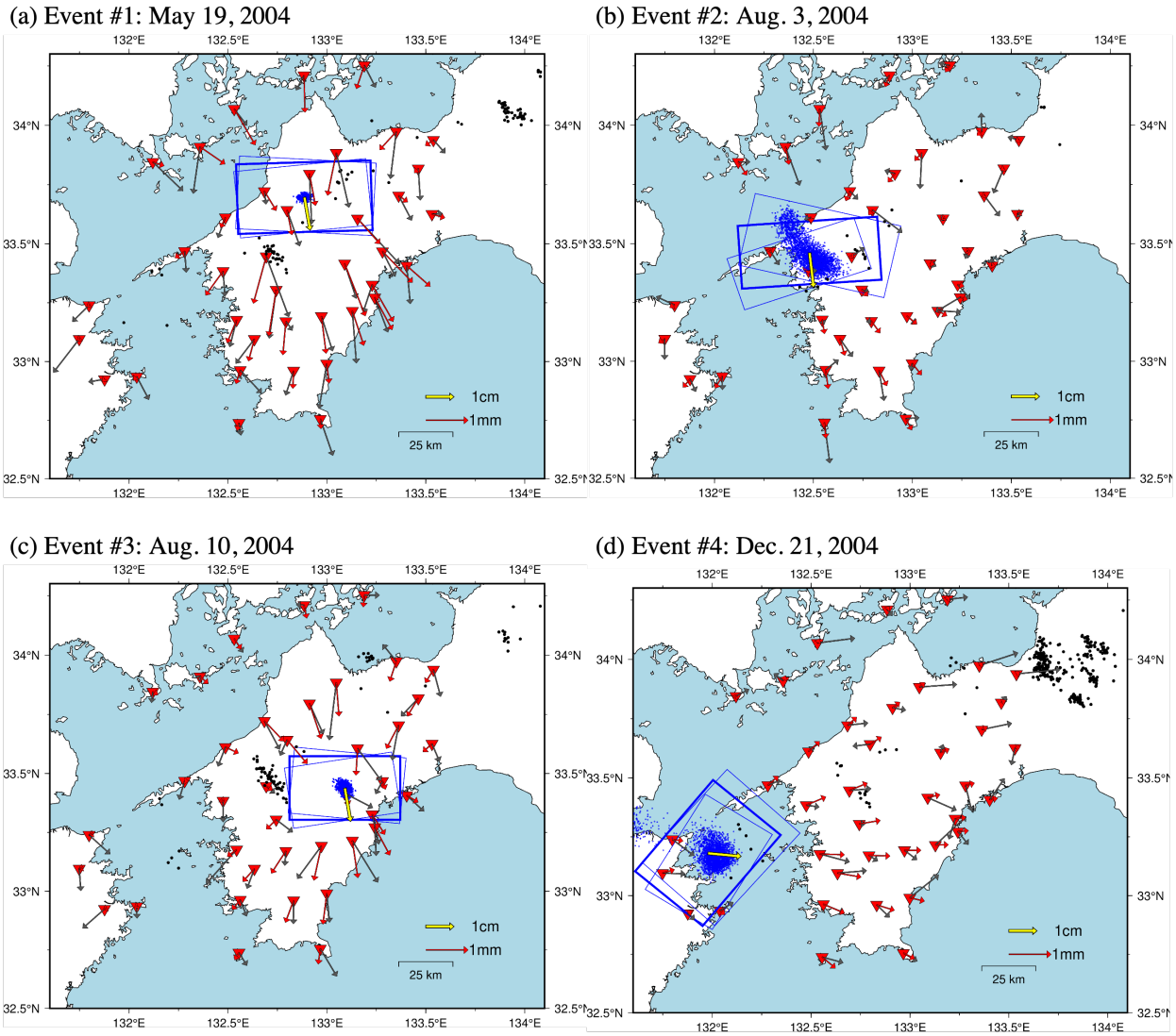

Figure 6. Inversion results of potential events detected with our method. In each figure, the gray and red arrows at a station (inverted red triangle) represent the observation and calculation using a rectangular fault model, respectively. Blue dots represent Markov chain Monte Carlo (MCMC) samples of the fault location. Black dots represent the epicenters of low-frequency earthquakes that occurred during the detection period ± 3 days. Blue rectangles with thick and thin frames denote rectangular faults calculated by the means and the 25% and 75% percentiles of the MCMC samples, respectively. The yellow arrow represents the slip vector calculated based on the mean of the MCMC samples.

Finally, we discuss the inversion results of the potential events detected by our

method. We conducted Markov chain Monte Carlo (MCMC; e.g., Hastings, 1970) using a rectangular fault model buried in an elastic half-space (Okada, 1992). For the detail of MCMC method, see supplemental file Text S1. We used the displacements at 39 stations three days after the detected day for the inversion process. Ten source parameters, i.e., longitude, latitude, depth, length, width, slip amount, rake, strike, dip, and dislocation of the tensile component, were determined. Figure 6 shows representative examples with different positions of fault locations and epicenters of LFEs that occurred during the detection period ± 3 days. The determined faults of these events (Figure 6) locate near the fault locations of known S-SSEs in this area (Figure 1b). The determined fault size, slip size, and depth are similar to those of known S-SSEs, and the determined rake suggests that these events have reverse faults (Figures S1-S4 in the supplemental file). Taking the uncertainty into consideration, the determined faults of these events cover the epicenters of LFEs, which might suggest the spatio-temporal co-occurrence of S-SSEs and LFEs.

6 Conclusion

We developed a new detection method for S-SSEs based on observations made by a GNSS array. Our method utilizes l_1 trend filtering, a variation of sparse estimation, in conjunction with combined p-value techniques. The results of synthetic tests show that almost all events were successfully detected by the proposed method, with few misdetections, compared to automated detection methods based on the AIC. We then applied the proposed method to the daily displacements obtained at 39 GNSS stations in the Nankai subduction zone, Southwest Japan. The results show that new potential events can be identified with the proposed method in addition to all known events detected by tiltmeters or GNSS. Finally, we discuss the correlation between these potential events and LFEs in the target region and inversion results.

Acknowledgments

The GEONET F3 solution available via the website of the Geospatial Information Authority of Japan (https://terras.gsi.go.jp) was used in the present study. The catalog created by Kato and Nakagawa (2020) was used for the discussion. The GMT software package (Wessel & Smith, 1998) was used to create the graphs. The Python wrapper of the Okada DC3D rectangular dislocation surface FORTRAN subroutine (https://github.com/tbenthompson/okada_wrapper) was used for the inversion. This work was supported by Japan Science and Technology Agency's Core Research for Evolutional Science and Technology (JST CREST) [grant Number JPMJCR1763] and by MEXT Project for Seismology toward Research Innovation with Data of Earthquake (STAR-E) [Grant Number JPJ010217].

References

Akaike, H. (1974). A new look at the statistical model identification. *IEEE Transactions on Automatic Control*, **19**, 716–723. https://doi.org/10.1109/TAC.1974.1100705

Ando, M. (1975). Source mechanisms and tectonic significance of historical earthquakes along the Nankai Trough, Japan. *Tectonophysics*, **27**, 119–140.

Baba, T., Tanioka, Y., Cummins, P. R., & Uhira, K. (2002). The slip distribution of the 1946 Nankai earthquake estimated from tsunami inversion using a new plate model. *Physics of the Earth and Planetary Interiors*, **132**, 59–73. https://doi.org/10.1016/S0031-9201(02)00044-4

Baba, T., Cummins, P. R., Hori, T., & Kaneda, Y. (2006). High precision slip distribution of the 1944 Tonankai earthquake inferred from tsunami waveforms: Possible slip on a splay fault. *Tectonophysics*, **426**, 119–134. https://doi.org/10.1016/j.tecto.2006.02.015

Bartlow, N. M., Miyazaki, S., Bradley, A. M., & Segall, P. (2011). Space-time correlation of slip and tremor during the 2009 Cascadia slow slip event. *Geophysical Research Letters*, **38**, L18309. https://doi.org/10.1029/2011GL048714

Bartlow, N. M. (2020). A long-term view of Episodic Tremor and Slip in Cascadia. *Geophysical Research Letters*, **47**, e2019GL085303. https://doi.org/10.1029/2019GL085303

Beroza, G. C., & Ide, S. (2011). Slow earthquakes and nonvolcanic tremor. *Annual Review of Earth Planetary Sciences*, **39**, 271–296. https://doi.org/10.1146/annurev-earth-040809-152531

Charlety, J., Voronin, S., Nolet, G., Loris, I., Simons, F. J., Sigloch, K., & Daubechies, I. C. (2013). Global seismic tomography with sparsity constraints: Comparison with smoothing and damping regularization. *Journal of Geophysical Research: Solid Earth*, **118**, 4887–4899.

Douglas, A., Beavan, J., Wallace, L., & Townend, J. (2005). Slow slip on the northern Hikurangi subduction interface, New Zealand. *Geophysical Research Letters*, **32**, L16305. https://doi.org/10.1029/2005GL023607

Dragert H., Wang K., & James, T. S. (2001). A silent slip event on the deeper subduction interface. *Science*, **292**, 5521, 1525–1528. https://doi.org/10.1126/science.1060152

Evans, E. L., & Meade, B. J. (2012). Geodetic imaging of coseismic slip and postseismic afterslip: Sparsity promoting methods applied to the great Tohoku earthquake. *Geophysical Research Letters*, **39**, L11314.

Frank, W. B., Radiguet, M., Rousset, B., Shapiro, N. M., Husker, A. L., Kostoglodov, V., Cotte, N., & Campillo, M. (2015). Uncovering the geodetic signature of silent slip through repeating earthquakes. *Geophysical Research Letters*, **42**, 2774–2779. https://doi.org/10.1002/2015GL063685

Fujita, M., Nishimura, T., & Miyazaki, S. (2019). Detection of small crustal deformation caused by slow slip events in southwest Japan using GNSS and

tremor data. *Earth, Planets and Space*, **71**, https://doi.org/10.1186/s40623-01901075-x

Good, I. J. (1958). Significance tests in parallel and in series. *Journal of the American Statistical Association*, **53**, 799–813. https://doi.org/10.1080/01621458.1958.10501480

Graham, S. E., Demets, C., Cabral-Cano, E., Kostoglodov, V., Walpersdorf, A., Cotte, N., Brudzinski, M., Mccaffrey, R., & Salazar-Tlaczani, L. (2014). GPS constraints on the 2011–2012 Oaxaca slow slip event that preceded the 2012 March 20 Ometepec earthquake, southern Mexico. *Geophysical Journal International*, **197**, 1593–1607. https://doi:10.1093/gji/ggu019

Hall, K., Houston, H., & Schmidt, D. (2018). Spatial comparisons of tremor and slow slip as a constraint on fault strength in the northern Cascadia subduction zone, *Geochemistry, Geophysics, Geosystems*, **19**, 2706–2718. https://doi.org/10.1029/2018GC007694

Hastings, W. K. (1970). Monte Carlo sampling methods using Markov chains and their applications, *Biometrika*, **57**, 97–109.

Hirose, H., Hirahara, K., Kimata, F., Fujii, N., & Miyazaki, S. (1999). A slow thrust slip event following the two 1996 Hyuganada earthquakes beneath the Bungo Channel, southwest Japan. *Geophysical Research Letters*, **26**, 3237–3240. https://doi.org/10.1029/1999GL010999

Hirose, H., & Obara, K. (2005). Repeating short- and long-term slow slip events with deep tremor activity around the Bungo channel region, southwest Japan. *Earth Planets Space*, **57**, 961–972. https://doi.org/10.1186/BF03351875

Hirose, T., Nakahara, H., Nishimura, T., & Campillo, M. (2020). Locating spatial changes of seismic scattering property by sparse modeling of seismic ambient noise cross-correlation functions: Application to the 2008 Iwate-Miyagi Nairiku (Mw 6.9), Japan, earthquake. *Journal of Geophysical Research: Solid Earth*, **125**, e2019JB019307.

Ito, Y., Hino, R., Kido, M, Fujimoto, H., Osada, Y., Inazu D., Ohta Y., Iinuma, T., Ohzono, M., Miura, S., Mishina, M., Suzuki, K., Tsuji, T., & Ashi, J. (2013). Episodic slow slip events in the Japan subduction zone before the 2011 Tohoku-Oki earthquake. *Tectonophysics*, **600**, 14–26. https://doi.org/10.1016/j.tecto.2012.08.022

Kano, M., Kato, A., & Obara, K. (2019). Episodic tremor and slip silently invades strongly locked megathrust in the Nankai Trough. *Scientific Reports*, **9**, 9270. https://doi.org/10.1038/s41598-019-45781-0

Kato, A., Obara, K., Igarashi T., Tsuruoka, H., Nakagawa, S., & Hirata, N. (2012). Propagation of slow slip leading up to the 2-11 Mw 9.0 Tohoku-Oki earthquake. *Science*, **10**, 705–708. https://doi.org/10.1126/science.1215141

Kato, A., & Nakagawa, S. (2020). Detection of deep low-frequency earthquakes in the Nankai subduction zone over 11 years using a matched filter technique. *Earth Planets Space*, **72**, 128. https://doi.org/10.1186/s40623-020-01257-4

Kim, S.-J., Koh, K., Boyd, S., & Gorinevsky, D. (2009). l_1 trend filtering. *SIAM Review*, **51**, 339–360.

Klinger, Y. (2010). Relation between continental strike-slip earthquake segmentation and thickness of the crust. *Journal of Geophysical Research: Solid Earth*, **115**, B07306. https://doi.org/10.1029/2009JB006550

Kostoglodov, V., Sing, S. K., Santiago, J. A., & Franco, S. I. (2003). A large silent earthquake in the Guerrero seismic gap, Mexico. *Geophysical Research Letters*, **30**, 1807. https://doi.org/10.1029/2003GL017219

Loris, I., Nolet, G., Daubechies, I., & Dahlen, F. A. (2007). Tomographic inversion using l1-norm regularization of wavelet coefficients. *Geophysical Journal International*, **170**, 359–370. https://doi.org/10.1111/j.1365-246X.2007.03409.x

Mallows, C. (1973). Some comments on C_p. *Technometrics*, **15**, 661–675.

Miller, M., Melbourne, T., Johnson, D., & Sumner, W. (2002). Periodic slow earthquakes from the Cascadia subduction zone. *Science*, **295**, 2423. https://doi.org/10.1126/science.1071193.

Nakagawa, H., Toyofuku, T., Kotani, K., Miyahara, B., Iwashita, C., Kawamoto, S., Hatanaka, Y., Munekane, H., Ishimoto, M., Yutsudo, T., Ishikura, N., & Sugawara, Y. (2009). Development and validation of GEONET new analysis strategy (Version 4). *Journal of Geospatial Information Authority of Japan*, **118**, 1–8 (in Japanese).

Nakata, R., Hino, H., Kuwatani, T., Yoshioka, S., Okada, M., & Hori, T. (2017). Discontinuous boundaries of slow slip events beneath the Bungo Channel, southwest Japan. *Scientific Reports*, **7**, 6129.

Nakata, R., Kuwatani, T., Okada, M., & Hori, T. (2016). Geodetic inversion for spatial distribution of slip under smoothness, dis- continuity, and sparsity constraints. *Earth, Planets and Space*, **68**, 20.

Nishimura, T., Matsuzawa, T., & Obara, K. (2013). Detection of short-term slow slip events along the Nankai Trough, southwest Japan, using GNSS data. *Journal of Geophysical Research: Solid Earth*, **118**, 3112–3125. https://doi.org/10.1002/jgrb.50222

Nishimura, T. (2014). Short-term slow slip events along the Ryukyu Trench, southwestern Japan observed by continuous GNSS. *Progress in Earth and Planetary Science,* **1**, 1—12. https://doi.org/10.1186/s40645-014-0022-5

Nishimura, T. (2020). Slow slip events in the Kanto and Tokai regions of central Japan detected using Global Navigation Satellite System data during 1994-2020. *Geochemistry, Geophysics, Geosystems*, **22**, e2020GC009329.

Obara, K., & Kato, A. (2016). Connecting slow earthquakes to huge earthquakes. *Science*, **353**, 253–257.

Obara, K., Hirose, H., Yamamizu, F., & Kasahara, K. (2004). Episodic slow slip events accompanied by non-volcanic tremors in southwest Japan subduction zone. *Geophysical Research Letters*, **31**. https://doi.org/10.1029/2004GL020848

Obara, K., & Sekine, S. (2009). Characteristic activity and migration of episodic tremor and slow-slip events in central Japan. *Earth, Planets and Space*, **61**, 853–862.

Ohta, Y., Freymueller, J. T., Hreinsdóttir, S., & Suito, H. (2006). A large slow slip event and the depth of the seismogenic zone in the southcentral Alaska subduction zone. *Earth Planetary Science Letters*, **247**, 108–116.

Okada, Y. (1992). Internal deformation due to shear and tensile fauls in a half-space. *Bulletin of the Seismological Society of America*, **82**, 1018–1040.

Ozawa, S., Murakami, M., Kaidzu, M. Tada, T., Sagiya, T, Hatanaka, Y., Yarai, H., & Nishimura, T. (2002). Detection and monitoring of ongoing aseismic slip in the Tokai region, central Japan. *Science*, **298**, 1009–1012.

Ozawa, S., Nishimura, T., Munekane, H., Suito, H., Kobayashi, T., Tobita, M., & Imakiire, T. (2012). Preceding, coseismic, and postseismic slips of the 2011 Tohoku earthquake, Japan. *Journal of Geophysical Research:Solid Earth*, **117**, B07404. https://doi.org/10.1029/2011JB009120

Payero, J. Kostoglodov, V., Shapiro, N., Mikumo, T., Iglesias, A., Pérez-Campos, X., & Clayton, R. (2008). Nonvolcanic tremor observed in the Mexican subduction zone. *Geophysical Research Letters*, **35**. https://doi.org/10.1029/2007GL032877

Radiguet, M., Perfettini, H., Cotte, N., Gualandi, A., Valette, B., Kostoglodov, V., Lhomme, T., Walpersdord, A., Cabral-Cano, E., & Campillo, M. (2016). Triggering of the 2014 M_{w}7.3 Papanoa earthquake by a slow slip event in Guerrero, Mexico. *Nature Geoscience*, **9**, 829–833. https://doi.org/10.1038/ngeo2817

Rousset, B., Campillo, M., Lasserre, C., Frank, W. B., Cotte, N., Walpersdorf, A., Socquet, A., & Kostoglodov, V. (2017). A geodetic matched filter search for slow slip with application to the Mexico subduction zone. *Journal of Geophysical Research: Solid Earth*, **122**, 498–514. https://doi.org/10.1002/2017JB014448

Ruiz, S., Metois, M., Fuenzalida, A., Ruiz, J., Leyton, F., Grandin, R., Vigny, C., Madariaga, R., & Campos, J. (2014). Intense foreshocks and a slow slip event preceded the 2014 Iquique Mw 8.1 earthquake. *Science*, **345**, 1165–1169.

Sagiya, T., & Thatcher, W. (1999). Coseismic slip resolution along a plate boundary megathrust: The Nankai Trough, southwest Japan. *Journal of Geophysical Research*, **104**, 1111–1129. https://doi.org/10.1029/98JB02644

Schwartz, S. Y., & Rokosky, J. M. (2007). Slow slip events and seismic tremor at circum-Pacific subduction zones. *Review of Geophysics*, **45**. https://doi.org/10.1029/2006RG000208

Socquet, A., Valdes, J. P., Jara, J., Cotton, F., Walpersdorf, A., Cotte, N., Specht, S., Ortega-Culaciati, F., Carrizo, D., & Norabuena, E. (2017). An 8 month slow slip event triggers progressive nucleation of the 2014 Chile megathrust. *Geophysical Research Letters*, **44**, 4046–4053. https://doi.org/10.1002/2017GL073023.

Tibshirani, R. J., & Taylor, J. (2012). Degrees of freedom in LASSO problems. *The Annals of Statistics*, **40**, 1198–1232.

Tibshirani, R. J. (2014). Adaptive piecewise polynomial estimation via trend filtering. *The Annals of Statistics*, **42**, 285–323.

Voss, N., Dixon, T. H., Liu, Z., Malservisi, R., Protti, M., & Schwartz, S. (2018) Do slow slip events trigger large and great earthquakes? *Science Advances*, **4**, eaat8472. https://doi.org/10.1126/sciadv.aat8472

Wallace, L. M., & Beavan, J. (2006) A large slow slip event on the central Hikurangi subduction interface beneath the Manawatu region, North Island, New Zealand. *Geophysical Research Letters*, **33**, L11301. https://doi.org/10.1029/2006GL026009

Wilson, D. J. (2019). The harmonic mean p-value for combining dependent tests. *Proceedings of the National Academy of Science*, **116**, 1195–1200.

Yao, H., Gerstoft, P., Shearer, P. M., & Mecklenbräuker, C. (2011). Compressive sensing of the Tohoku-Oki Mw 9.0 earthquake: Frequency-dependent rupture modes. *Geophysical Research Letters*, **38**, L20310.

Yokota, Y., & Koketsu, K. (2015). A very long-term transient event preceding the 2011 Tohoku earthquake. *Nature Communications*, **6**, 5934. https://doi.org/10.1038/ncomms6934